JAERI-M
8517

POLOIDAL DISTRIBUTIONS OF NEUTRON FLUX, RADIATION DAMAGE AND NUCLEAR HEATING RATE IN A FIRST WALL SYSTEM OF INTOR-J

October 1979

Hiromasa IIDA, Yasushi SEKI
Takashi YAMAMOTO[*1] and Hiromitsu KAWASAKI[*2]

日本原子力研究所
Japan Atomic Energy Research Institute

JAERI-M 8517

Poloidal Distributions of Neutron Flux, Radiation Damage and Nuclear Heating Rate in a First Wall System of INTOR-J

H. IIDA, Y. SEKI, T. YAMAMOTO[*1]
and H. KAWASAKI[*2]

Division of Thermonuclear Fusion Research
Tokai Research Establishment, JAERI

(Received September 29, 1979)

Poloidal distributions of neutron flux, radiation damage rate and nuclear heating rate in a first wall and a protection wall of INTOR-J are calculated using three-dimensional Monte Carlo transport code. The peaking factors of 14 MeV neutron flux and helium production rate are about 1.3 and those of DPA and nuclear heating rate are about 1.2.

Keywords: INTOR-J Fusion Reactor, Poloidal Distribution, 14 MeV Neutron Flux, Nuclear Heating Rate, Helium Production Rate, Displacement Damage Rate, Monte Carlo Transport Code, Peaking Factor, Radiation Damage

---

*1 On leave from Fuji Electric Co. Ltd.
*2 Century Research Center Corporation

JAERI－M 8517

INTOR－J 第1壁の中性子束，放射線損傷および放射線発熱分布

日本原子力研究所東海研究所核融合研究部
飯田浩正・関　泰・山本　孝[*1]・川崎弘光[*2]

（1979年9月29日受理）

3次元モンテカルロ計算コードを用いて，INTOR－J 第1壁の中性子束，放射線損傷率，放射線発熱のポロイダル方向分布を求めた。14 MeV 中性子束とヘリウム生成率の分布のピーキングファクタは約1.3，DPA及び放射線発熱のピーキングファクタは約1.2となった。

*1 外来研究員：富士電気製造K。K。

*2 センチュリー・リサーチ・センター（株）

CONTENTS

目　　次

INTRODUCTION

INTOR-J[1] is a Japanese proposal for INTOR (IAEA Tokamak Reactor) which is a compact size tokamak reactor with a non-circular cross section plasma. In this report, poloidal distributions of 14 MeV neutron fluxes and rates of helium production, displacement and nuclear heating in a first wall system are calculated using a three-dimensional Monte Carlo transport code.

Blanket test sections will be installed to INTOR for tritium breeding and materials irradiation tests. Their positions in poloidal direction should be chosen to attain the highest neutron fluence and radiation damage rate.

Heat removal from first wall is one of crucial problems of a first wall system design for tokamak reactor with high wall loading. Evaluation of nuclear heating distribution is required for a realistic thermal design of the first wall system.

The poloidal distribution of neutron flux in a first wall of tokamak reactor with circular cross section plasma has been calculated by several authors[2)~6)] using the ray-tracing method or Sn transport code. Monte Carlo method is not necessarily required when plasma and first wall are circular[7)]. However in case of INTOR-J with non-circular plasma cross section Monte Carlo method seems to be the only choice.

INTOR-J CONFIGURATION

Depending on the method of ash exhaust, there are a concept with poloidal divertor and one without for INTOR-J reactor configuration. In this paper the former case is investigated. Figure 1 shows a side view of INTOR-J blanket concept. This concept has a tritium breeding blanket on the outboard of torus. The following calculation is made based on this figure.

The first wall system of INTOR-J consists of the closest part of blanket to plasma (the first wall) and a protection wall in front of it. The blanket structure and the protection wall are made with stainless steel and molybdenum alloy, respectively.

INTRODUCTION

INTOR-J[1] is a Japanese proposal for INTOR (IAEA Tokamak Reactor) which is a compact size tokamak reactor with a non-circular cross section plasma. In this report, poloidal distributions of 14 MeV neutron fluxes and rates of helium production, displacement and nuclear heating in a first wall system are calculated using a three-dimensional Monte Carlo transport code.

Blanket test sections will be installed to INTOR for tritium breeding and materials irradiation tests. Their positions in poloidal direction should be chosen to attain the highest neutron fluence and radiation damage rate.

Heat removal from first wall is one of crucial problems of a first wall system design for tokamak reactor with high wall loading. Evaluation of nuclear heating distribution is required for a realistic thermal design of the first wall system.

The poloidal distribution of neutron flux in a first wall of tokamak reactor with circular cross section plasma has been calculated by several authors[2)~6)] using the ray-tracing method or Sn transport code. Monte Carlo method is not necessarily required when plasma and first wall are circular[7)]. However in case of INTOR-J with non-circular plasma cross section Monte Carlo method seems to be the only choice.

INTOR-J CONFIGURATION

Depending on the method of ash exhaust, there are a concept with poloidal divertor and one without for INTOR-J reactor configuration. In this paper the former case is investigated. Figure 1 shows a side view of INTOR-J blanket concept. This concept has a tritium breeding blanket on the outboard of torus. The following calculation is made based on this figure.

The first wall system of INTOR-J consists of the closest part of blanket to plasma (the first wall) and a protection wall in front of it. The blanket structure and the protection wall are made with stainless steel and molybdenum alloy, respectively.

ONE DIMENSIONAL CALCULATION

Because of noncircular cross section of plasma and nonuniformity of blanket, it is not possible to make accurate calculation model of INTOR-J with one dimensional transport code. And the normalization of neutron source intensity becomes a problem. Two ways for the normalization can be considered ; Fusion Power Normalization and Wall Loading Normalization. Figure 2 shows the schematic layout of out board calculational model of INTOR-J. In one-dimensional Sn transport code ANISN, the height of cylinder is taken to be 1 cm. The fusion power in the disc of INTOR-J plasma with 1 cm thickness corresponding to the calculational model is 0.1257 MW. The first way to normalize the source intensity is to let the fusion power in the calculational model equal to 0.1257 MW (Fusion Power Normalization). On the other hand, the surface area of first wall in the calculational model is 0.08482 m^2. The second way for the normalization is to equate the fusion power in the calculational model to 0.1060 MW considering that the wall loading of INTOR-J is 1.25 MW/m^2 (Wall Loading Normalization). In the former case we will obtain the value near the maximum in poloidal direction. In the latter the calculated value will be near the average. In any case the meaning of the results obtained from one dimensional calculation is vague.

Table 1 and 2 show 42-group neutron and 21-gamma energy structures, respectivly.

Helium production and displacement cross sections of stainless steel and molybdenum are shown in tables 3 and 4.

The result of the ANISN calculation is shown in Table 5.

NEUTRON SOURCE DISTRIBUTION IN THREE DIMENSIONAL CALCULATION

Neutrons are emitted isotropically from sources distributed proportional to the fusion power density.

The power density distribution is obtained by the following process. In the MHD equilibrium, plasma pressure is expressed with the flux function Ψ as follows:

$$P = P_0 \, \psi^{\zeta}$$

ONE DIMENSIONAL CALCULATION

Because of noncircular cross section of plasma and nonuniformity of blanket, it is not possible to make accurate calculation model of INTOR-J with one dimensional transport code. And the normalization of neutron source intensity becomes a problem. Two ways for the normalization can be considered ; Fusion Power Normalization and Wall Loading Normalization. Figure 2 shows the schematic layout of out board calculational model of INTOR-J. In one-dimensional Sn transport code ANISN, the height of cylinder is taken to be 1 cm. The fusion power in the disc of INTOR-J plasma with 1 cm thickness corresponding to the calculational model is 0.1257 MW. The first way to normalize the source intensity is to let the fusion power in the calculational model equal to 0.1257 MW (Fusion Power Normalization). On the other hand, the surface area of first wall in the calculational model is 0.08482 m^2. The second way for the normalization is to equate the fusion power in the calculational model to 0.1060 MW considering that the wall loading of INTOR-J is 1.25 MW/m^2 (Wall Loading Normalization). In the former case we will obtain the value near the maximum in poloidal direction. In the latter the calculated value will be near the average. In any case the meaning of the results obtained from one dimensional calculation is vague.

Table 1 and 2 show 42-group neutron and 21-gamma energy structures, respectivly.

Helium production and displacement cross sections of stainless steel and molybdenum are shown in tables 3 and 4.

The result of the ANISN calculation is shown in Table 5.

NEUTRON SOURCE DISTRIBUTION IN THREE DIMENSIONAL CALCULATION

Neutrons are emitted isotropically from sources distributed proportional to the fusion power density.

The power density distribution is obtained by the following process. In the MHD equilibrium, plasma pressure is expressed with the flux function Ψ as follows:

$$P = P_0 \, \psi^{\zeta}$$

Then ion temperature and density distributions are assumed as follows:

$$T = T_0 \, \psi^{\eta}$$

$$n = n_0 \, \psi^{\xi}$$

$$\eta + \xi = \zeta$$

In the case of INTOR, the value of ζ is 1.48, and η is assumed to be 1.0 for this calculation.

The fusion power density is given by

$$P_f = \frac{< \sigma v > n^2}{4} \cdot Q$$

Figure 3 shows the fusion power density distribution when the average ion temperature $\bar{T}$ is 10 keV. Where $\bar{T}$ is defined as

$$\bar{T} = \frac{\int nT \, dv}{\int n \, dv}$$

The fusion reaction cross section used in this calculation is

$$< \sigma v > = 370.0 \exp(-20 \times Ti^{-\frac{1}{3}}) \; / \; ((1+(Ti/70)^{1.3}) \times Ti^{\frac{2}{3}}) \quad 8)$$

THREE-DIMENSIONAL CALCULATION

The Monte Carlo transport Code MORSE-I[9] and input debugging code TOPIC[10] are used in three-dimensional calculation. Brief descriptions of MORSE-I and TOPIC are given in Appendix. Figure 4 shows a three-dimensional calculation model of INTOR-J.

Thirty-two energy group P_5 cross section set is employed. Neutron and gamma energy group structures are shown in tables 6 and 7. Tables 8, 9 and 10 show 32 group KERMA (Kinetic Energy Released in Materials) factor, displacement cross sections and helium production cross sections, respectively. These cross sections are obtained being collapsed from 63 group cross sections with the aid of one dimensional calculations.

The number of histories followed is 11600. It requires computational time of about 10 hours with FACOM 230/75 system.

Then ion temperature and density distributions are assumed as follows:

$$T = T_0 \, \psi^{\eta}$$

$$n = n_0 \, \psi^{\xi}$$

$$\eta + \xi = \zeta$$

In the case of INTOR, the value of ζ is 1.48, and η is assumed to be 1.0 for this calculation.

The fusion power density is given by

$$P_f = \frac{< \sigma v > n^2}{4} \cdot Q$$

Figure 3 shows the fusion power density distribution when the average ion temperature $\bar{T}$ is 10 keV. Where $\bar{T}$ is defined as

$$\bar{T} = \frac{\int nT \, dv}{\int n \, dv}$$

The fusion reaction cross section used in this calculation is

$$< \sigma v > = 370.0 \exp(-20 \times Ti^{-\frac{1}{3}}) \; / \; ((1+(Ti/70)^{1.3}) \times Ti^{\frac{2}{3}}) \quad 8)$$

THREE-DIMENSIONAL CALCULATION

The Monte Carlo transport Code MORSE-I[9] and input debugging code TOPIC[10] are used in three-dimensional calculation. Brief descriptions of MORSE-I and TOPIC are given in Appendix. Figure 4 shows a three-dimensional calculation model of INTOR-J.

Thirty-two energy group P_5 cross section set is employed. Neutron and gamma energy group structures are shown in tables 6 and 7. Tables 8, 9 and 10 show 32 group KERMA (Kinetic Energy Released in Materials) factor, displacement cross sections and helium production cross sections, respectively. These cross sections are obtained being collapsed from 63 group cross sections with the aid of one dimensional calculations.

The number of histories followed is 11600. It requires computational time of about 10 hours with FACOM 230/75 system.

RESULTS AND DISCUSSIONS

Both the protection wall and first wall are divided into eighteen regions as shown in Fig.5. Neutron and gamma fluxes averaged in each region are calculated using track-length estimator. The fluxes and rates of helium production, displacement damage and nuclear heating are shown in Fig.6~13.

Real curves in the figure are the least square fittings using 5th or 6th degree polynominal with the following limitations.

$$\frac{d}{d\theta} f(\theta) \Big/_{\theta=0^\circ} = 0$$

$$\frac{d}{d\theta} f(\theta) \Big/_{\theta=180^\circ} = 0$$

These limitations must be satisfied because a symmetrical boundary is assumed at the mid-plane. The peaking factors of 14 MeV neutron flux and helium production rate distributions are about 1.3 which is a little larger than those of DPA and nuclear heating rate distributions.

Because of the above limitations the fitting curves do not agree well with the original values at the innermost part ($\theta = 0^\circ$). It is necessary to make fractional standard deviations smaller for obtaining more accurate information about the flux at the innermost part. However it is practically impossible to follow more neutron histories because of increasing computational time.

The results of three-dimensional calculation are a little smaller than those of one-dimensional calculation. This may be caused by the overestimation of grazing component of particle flux in one dimensional calculation. Infinite cylinder approximation and uniform source distribution approximation overestimated the grazing component of particle flux.

ACKNOWLEDGMENT

The authors deeply thank Dr. K. Sako for his encouragement.

RESULTS AND DISCUSSIONS

Both the protection wall and first wall are divided into eighteen regions as shown in Fig.5. Neutron and gamma fluxes averaged in each region are calculated using track-length estimator. The fluxes and rates of helium production, displacement damage and nuclear heating are shown in Fig.6~13.

Real curves in the figure are the least square fittings using 5th or 6th degree polynominal with the following limitations.

$$\frac{d}{d\theta} f(\theta) \Big/_{\theta=0^\circ} = 0$$

$$\frac{d}{d\theta} f(\theta) \Big/_{\theta=180^\circ} = 0$$

These limitations must be satisfied because a symmetrical boundary is assumed at the mid-plane. The peaking factors of 14 MeV neutron flux and helium production rate distributions are about 1.3 which is a little larger than those of DPA and nuclear heating rate distributions.

Because of the above limitations the fitting curves do not agree well with the original values at the innermost part ($\theta = 0^\circ$). It is necessary to make fractional standard deviations smaller for obtaining more accurate information about the flux at the innermost part. However it is practically impossible to follow more neutron histories because of increasing computational time.

The results of three-dimensional calculation are a little smaller than those of one-dimensional calculation. This may be caused by the overestimation of grazing component of particle flux in one dimensional calculation. Infinite cylinder approximation and uniform source distribution approximation overestimated the grazing component of particle flux.

ACKNOWLEDGMENT

The authors deeply thank Dr. K. Sako for his encouragement.

REFERENCES

(1) K. Sako et al. : "Engineering Aspects of the JAERI Proposal for INTOR" JAERI-M 8503 (1979)

(2) W. Dänner : "Neutron Flux Asymmetry in Toroidal Geometries", IPP 4/101 (1972)

(3) W.G. Price, Jr. and D.L. Chapin : "Neutron Wall Load Distributions in a Circular Cross Section Tokamak", MATT-1102 (1975)

(4) D.L. Chapin and W.G. Price, Jr. : "A Comparison of the D-T Neutron Wall Load Distributions in Several Tokamak Fusion Reactor Designs", MATT-1186 (1975)

(5) M. Kasai, S. Kondo and S. An : "Poloidal Distribution of Radiation Heating and 14 MeV Neutron Flux at the First Wall", Proc. 9th Symp. on Fusion Technology, Garmisch-Partenkirchen, 1976 June 14-18 p.657-653 (1977)

(6) J. Jung : "Finite Difference Equations for Transport Calculation in Toroidal Geometry", Nucl. Sci. Eng., 60, 74 (1976)

(7) Y. Seki and H. Iida : to be published

(8) W. Horton Jr. and T. Kammash, Nuclear Fusion 13, (1973) 753

(9) H. Iida and M. Yamauchi : Proc. 1978 Fall Meeting of the Atomic Energy Soc. of Japan, B35 (1978) (in Japanese)

(10) H. Iida and H. Kawasaki : "TOPIC : A Debugging Code for Torus Geometry Input Data of Monte Carlo Transport Code", JAERI-M 8289 (1979) (in Japanese)

(11) E.A. Straker et al. : "The MORSE Code - A Multigroup Neutron and Gamma-Ray Monte Carlo Transport Code", ORNL-4585 (1970)

APPENDIX

I. MORSE-I

This code is a revision of the MORSE-GG code[11]. The following improvements are made.

I-1. MORSE-I can treat a torus geometry which is represented by using surface of fourth order while original MORSE-GG treats those which can be represented by surfaces of second order. The number of surfaces allowed in a block is increased from 17 to 35.

I-2. Point-detector technique is improved

I-2-1. Computational time required is reduced significantly by the Score Point Selection technique.

I-2-2. Specular reflection boundaries can be used as symmetric boundaries. Proper usage of this boundary also reduces computational time practically.

I-2-3. Infinite varience is eliminated by the Small Density Perturbation technique.

II. TOPIC

This code has the following features: (1) It debugs the geometry input data of not only MORSE-GG but also MORSE-I. (2) Its calculation results are shown in figures drawn by Plotter or COM, and the regions not defined or doubly defined are easily detected. (3) It finds a multitude of input data errors in a single run. (4) the input data required in this code are few, so that it is readily usable in a time sharing system of FACOM 230-60/75 computer.

Table 1 42-Group neutron energy group structure

Group	Energy Limits			Mid-Point Energy	
1	15.000	- 13.720	MeV	14.360	MeV
2	13.720	- 12.549		13.135	
3	12.549	- 11.478		12.014	
4	11.478	- 10.500		10.989	
5	10.500	- 9.314		9.907	
6	9.314	- 8.261		8.788	
7	8.261	- 7.328		7.795	
8	7.328	- 6.500		6.914	
9	6.500	- 5.757		6.129	
10	5.757	- 5.099		5.428	
11	5.099	- 4.516		4.808	
12	4.516	- 4.000		4.258	
13	4.000	- 3.162		3.581	
14	3.162	- 2.500		2.831	
15	2.500	- 1.871		2.186	
16	1.871	- 1.400		1.636	
17	1.400	- 1.058		1.229	
18	1.058	- 0.800		0.929	
19	0.800	- 0.566		0.683	
20	0.566	- 0.400		0.483	
21	0.400	- 0.283		0.342	
22	0.283	- 0.200		0.242	
23	0.200	- 0.141		0.171	
24	0.141	- 0.100		0.121	
25	100.0	- 46.5	KeV	73.25	KeV
26	46.5	- 21.5		34.0	
27	21.5	- 10.0		15.75	
28	10.0	- 4.65		7.325	
29	4.65	- 2.15		3.40	
30	2.15	- 1.00		1.575	
31	1.00	- 0.465		0.733	
32	0.465	- 0.215		0.340	
33	0.215	- 0.100		0.158	
34	100.0	- 46.5	eV	73.25	eV
35	46.5	- 21.5		34.0	
36	21.5	- 10.0		15.75	
37	10.0	- 4.65		7.325	
38	4.65	- 2.15		3.40	
39	2.15	- 1.00		1.58	
40	1.00	- 0.465		0.733	
41	0.465	- 0.215		0.340	
42	0.215	- 0.001		0.108	

Table 2 21-group neutron energy group structure

Group	Energy Limits (MeV)			Mid-Point Energy (MeV)
1	14.0	-	12.0	13.0
2	12.0	-	10.0	11.0
3	10.0	-	8.0	9.0
4	8.0	-	7.5	7.75
5	7.5	-	7.0	7.25
6	7.0	-	6.5	6.75
7	6.5	-	6.0	6.25
8	6.0	-	5.5	5.75
9	5.5	-	5.0	5.25
10	5.0	-	4.5	4.75
11	4.5	-	4.0	4.25
12	4.0	-	3.5	3.75
13	3.5	-	3.0	3.25
14	3.0	-	2.5	2.75
15	2.5	-	2.0	2.25
16	2.0	-	1.5	1.75
17	1.5	-	1.0	1.25
18	1.0	-	0.4	0.7
19	0.4	-	0.2	0.3
20	0.2	-	0.1	0.15
21	0.1	-	0.01	0.055

Table 3 42-Group helium production cross section (barns)

Neutron Energy Group	S.S.	Mo
1	7.938-2	9.120-2
2	6.993-2	6.343-2
3	5.814-2	3.793-2
4	4.618-2	2.500-2
5	3.189-2	1.570-2
6	1.767-2	8.800-3
7	8.875-3	4.700-3
8	4.607-3	2.550-3
9	2.253-3	1.440-3
10	9.218-4	7.900-4
11	2.250-4	4.400-4
12	1.094-4	2.500-4
13	6.011-6	0.0
14~42	0.0	0.0

Table 4 42-Group displacement cross section (barns)

Neutron Energy Group	S.S.	Mo
1	2573.0	1564.0
2	2474.0	1478.0
3	2354.0	1408.0
4	2320.0	1299.0
5	2221.0	1199.0
6	2087.0	1063.0
7	2016.0	981.0
8	2016.0	920.0
9	1969.0	908.0
10	1929.0	858.0
11	1843.0	792.0
12	1633.0	768.0
13	1417.0	778.0
14	1162.0	782.0
15	887.0	666.0
16	681.0	566.0
17	427.0	456.0
18	346.0	395.0
19	373.0	357.0
20	363.0	302.0
21	240.0	255.0
22	217.0	195.0
23	239.0	143.0
24	128.0	135.0
25	109.0	61.5
26	102.0	29.6
27	32.5	14.2
28	26.5	6.95
29	9.90	2.72
30	5.18	1.61
31	0.13	1.78
32	0.18	2.25
33	0.29	5.25
34	0.43	2.52
35	0.66	14.5
36	0.67	1.12
37	0.95	0.29
38	1.38	0.41
39	2.04	0.57
40	2.99	0.83
41	4.38	1.23
42	12.3	3.50

Table 5(a) The results of one-dimensional calculation (Fusion Power Normalization)

	Protection Wall	First Wall
Material	Mo alloy	S.S.
14 MeV Neutron Flux ($n/cm^2 \cdot s$)	6.352×10^{13}	8.859×10^{13}
Helium Production Rate (appm/s)	5.648×10^{-6}	8.533×10^{-6}
Displacement per Atom (/s)	3.016×10^{-7}	2.442×10^{-7}
Nuclear Heating Rate (w/cc)	10.58	9.203

Table 5(b) The results of one-dimensional calculation (Wall Loading Normalization)

	Protection Wall	First Wall
Material	Mo alloy	S.S.
14 MeV Neutron Flux ($n/cm^2 \cdot s$)	7.471×10^{13}	5.357×10^{13}
Helium Production Rate (appm/s)	7.196×10^{-6}	4.763×10^{-6}
Displacement per Atom (/s)	2.060×10^{-7}	2.543×10^{-7}
Nuclear Heating Rate (w/cc)	7.761	8.922

Table 6　22-Group neutron energy group structure

Neutron Group	Energy Limits	Mid-Point Energy
1	15.000 - 13.720 MeV	14.36 MeV
2	13.720 - 11.478	12.599
3	11.478 - 9.314	10.396
4	9.314 - 7.328	8.321
5	7.328 - 5.757	6.5425
6	5.757 - 4.516	5.1365
7	4.516 - 3.162	3.839
8	3.162 - 1.871	2.5165
9	1.871 - 1.058	1.4645
10	1.058 - 0.566	0.812
11	0.566 - 0.283	0.4245
12	0.283 - 0.141	0.212
13	0.141 - 0.0465	0.09375
14	46.5 - 10.0 KeV	28.25 KeV
15	10.0 - 2.15	6.075
16	2.15 - 0.465	1.3075
17	0.465 - 0.1	0.2825
18	100.0 - 21.5 eV	60.75 eV
19	21.5 - 4.65	13.075
20	4.65 - 1.00	2.825
21	1.00 - 0.215	0.6075
22	0.215 - 0.001	0.108

Table 7　10-Group gamma energy group structure

Gamma Group	Energy Limits(MeV)	Mid-Point Energy
1	14.0 - 10.0	12.0
2	10.0 - 7.5	8.75
3	7.5 - 6.5	7.0
4	6.5 - 5.5	6.0
5	5.5 - 4.5	5.0
6	4.5 - 3.5	4.0
7	3.5 - 2.5	3.0
8	2.5 - 1.5	2.0
9	1.5 - 0.4	0.95
10	0.4 - 0.01	0.205

Table 8 22-Group neutron KERMA factor

(Mev/cm)

Neutron Group	S.S.	Mo
1	0.3066	0.3087E-1
2	0.2735	0.2780E-1
3	0.1787	0.2214E-1
4	0.1111	0.1854E-1
5	0.7191E-1	0.1620E-1
6	0.4822E-1	0.1369E-1
7	0.3039E-1	0.1170E-1
8	0.1732E-1	0.9300E-2
9	0.9524E-2	0.6519E-2
10	0.5184E-2	0.4701E-2
11	0.3356E-2	0.3277E-2
12	0.2327E-2	0.2195E-2
13	0.1190E-2	0.9316E-3
14	0.8132E-3	0.2944E-3
15	0.1800E-3	0.7793E-4
16	0.4344E-4	0.4937E-4
17	0.1131E-4	0.5836E-4
18	0.7204E-5	0.6917E-4
19	0.8410E-5	0.1307E-4
20	0.1613E-4	0.8781E-5
21	0.3317E-4	0.1731E-4
22	0.9453E-4	0.4949E-4

Table 9 10-Group gamma-ray KERMA factor

(MeV/cm)

Gamma Group	S.S.	Mo
1	0.2025E+1	0.3117E+1
2	0.1467E+1	0.2200E+1
3	0.1203E+1	0.1760E+1
4	0.1025E+1	0.1473E+1
5	0.8421	0.1180E+1
6	0.6793	0.9183
7	0.5203	0.6738
8	0.3714	0.4657
9	0.2181	0.2886
10	0.1140	0.2907

Table 10 22-Group displacement cross section

(barn)

Neutron Group	S.S.	Mo
1	2.573+3	1.564+3
2	2.444+3	1.460+3
3	2.264+3	1.241+3
4	2.049+3	1.019+3
5	1.991+3	9.137+2
6	1.885+3	8.241+2
7	1.486+3	7.748+2
8	9.915+2	7.112+2
9	5.464+2	5.081+2
10	3.620+2	3.724+2
11	3.001+2	2.782+2
12	2.256+2	1.744+2
13	1.174+2	9.397+1
14	8.823+1	2.654+1
15	2.215+1	5.872
16	4.566	1.626
17	1.967	2.536
18	0.484	3.591
19	0.757	0.835
20	1.579	0.458
21	3.409	0.949
22	1.230+1	3.500

Table 11 22-Group helium production cross section

(barn)

Neutron Group	S.S.	Mo
1	7.938-2	9.120-2
2	6.697-2	5.680-2
3	3.816-2	1.963-2
4	1.292-2	6.584-3
5	3.358-3	1.963-3
6	5.616-4	6.101-4
7	3.889-5	8.136-5
8~22	0.0	0.0

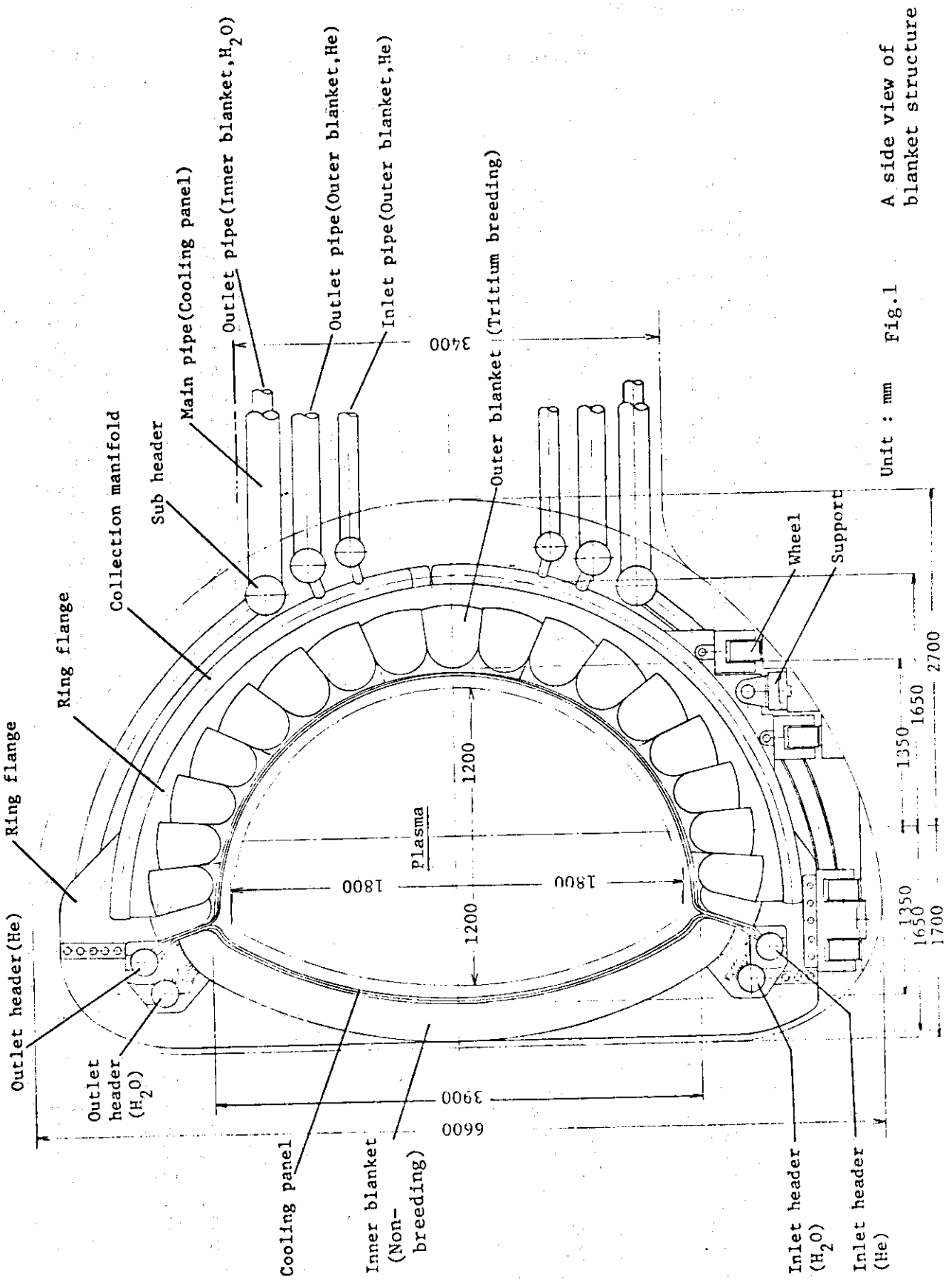

Unit : mm

Fig.1 A side view of blanket structure

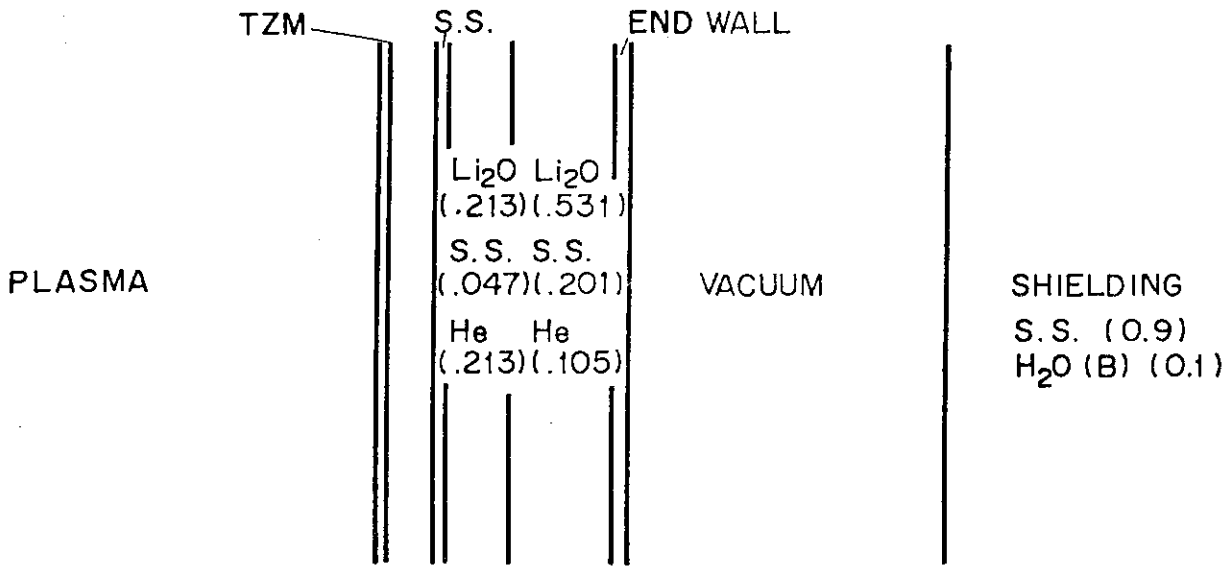

Fig.2 One-dimensional Calculation Model of INTOR-J

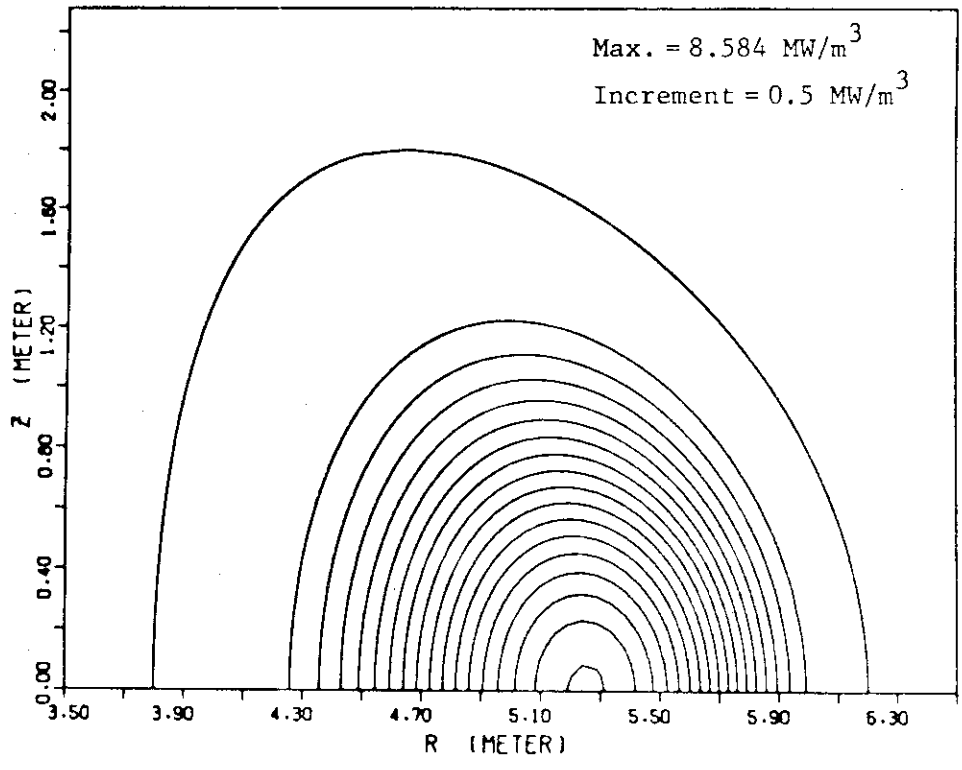

Fig.3 Power density contour

1 Vacuum
2 Protection wall
3 First wall
4 S.S. (0.8)+H_2O (0.2)
5 S.S. (0.9)+H_2O (0.1)
6 Li_2O (0.213)+S.S.(0.047)
+He (0.213)
7 Li_2O (0.5305)+S.S.(0.2015)
+He (0.105)
8 End wall
9 Inner shield
10 Outer shield

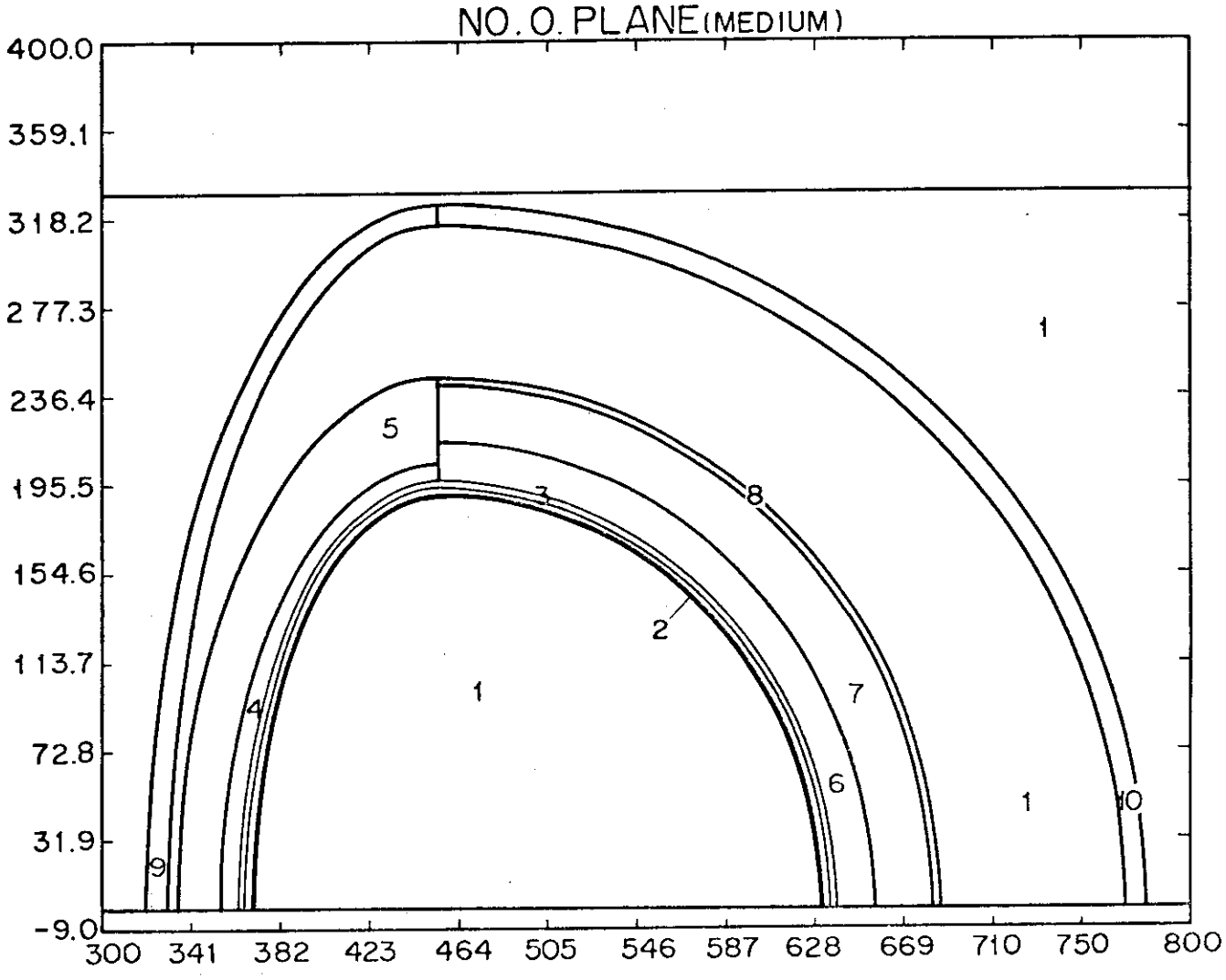

Fig.4 Three-dimensional Calculation Model of INTOR-J

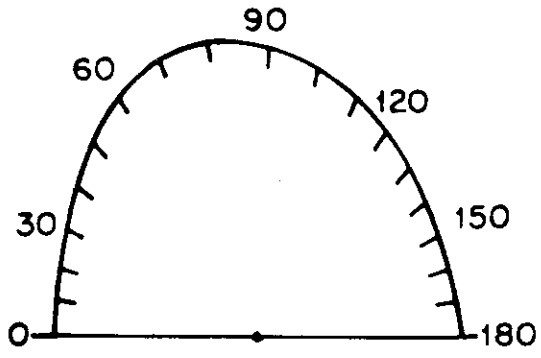

Fig. 5 Editting regions of the protection wall and the first wall

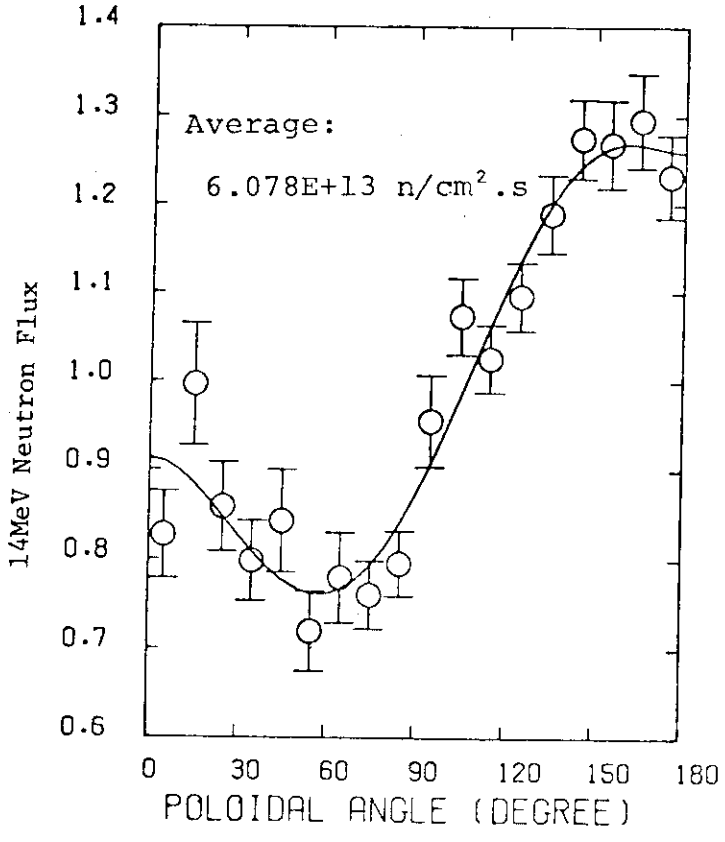

Fig.6 Poloidal distribution of 14MeV Neutron Flux in the Protection Wall

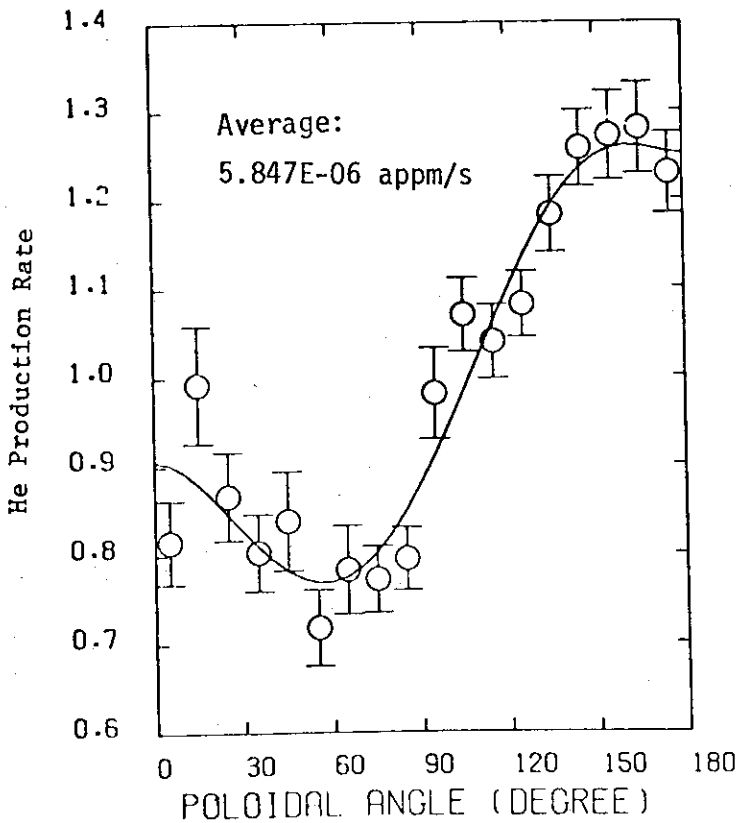

Fig.7 Poloidal distribution of Helium Production Rate in the Protection Wall

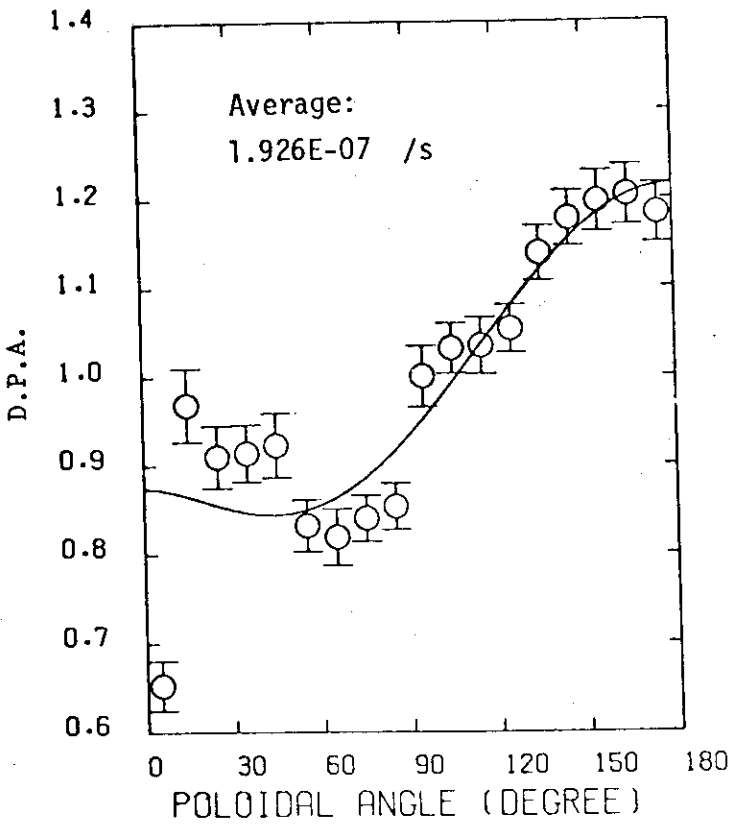

Fig.8 Poloidal distribution of D.P.A. in the Protection Wall

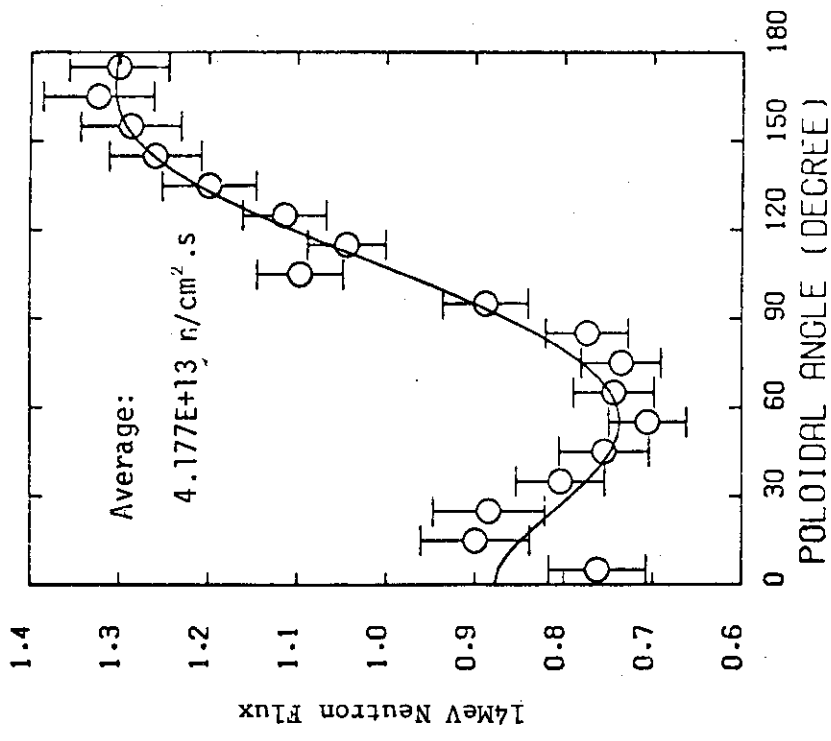

Fig.10 Poloidal distribution of 14MeV Neutron Flux in the First Wall

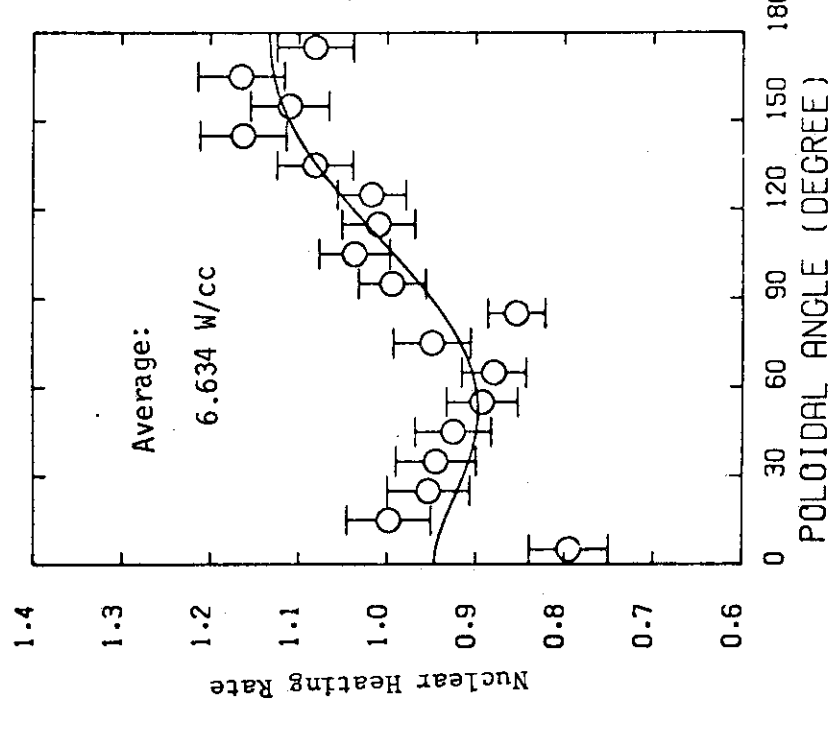

Fig.9 Poloidal distribution of Nuclear Heating Rate in the Protection Wall

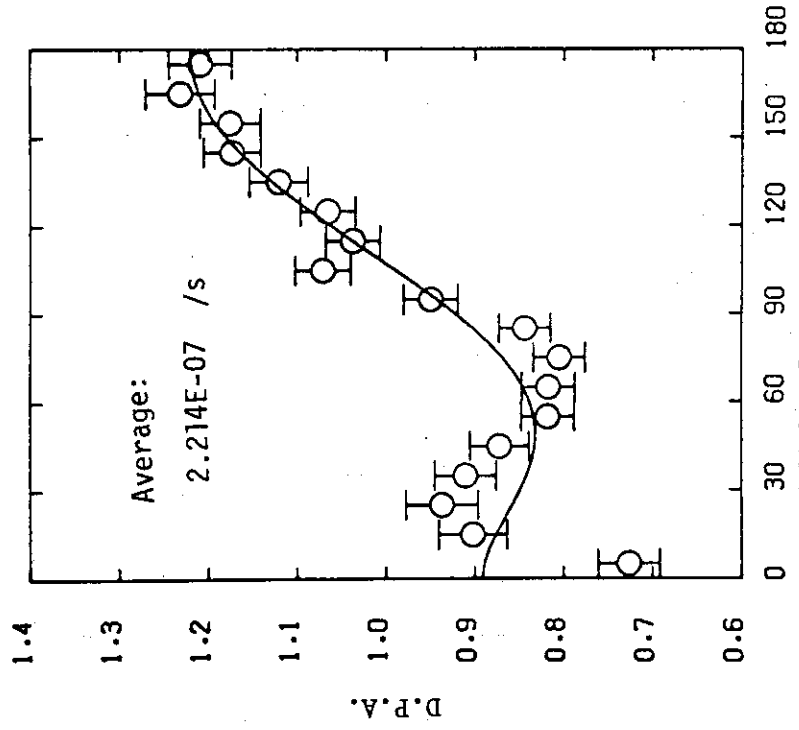

Fig.12 Poloidal distribution of D.P.A. in the First Wall

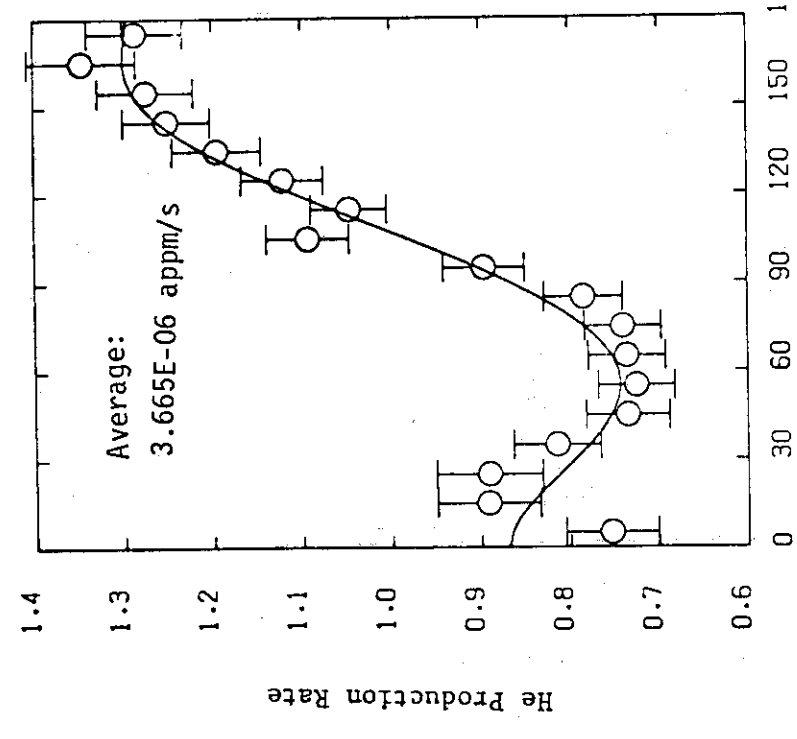

Fig.11 Poloidal distribution of Helium Production Rate in the First Wall

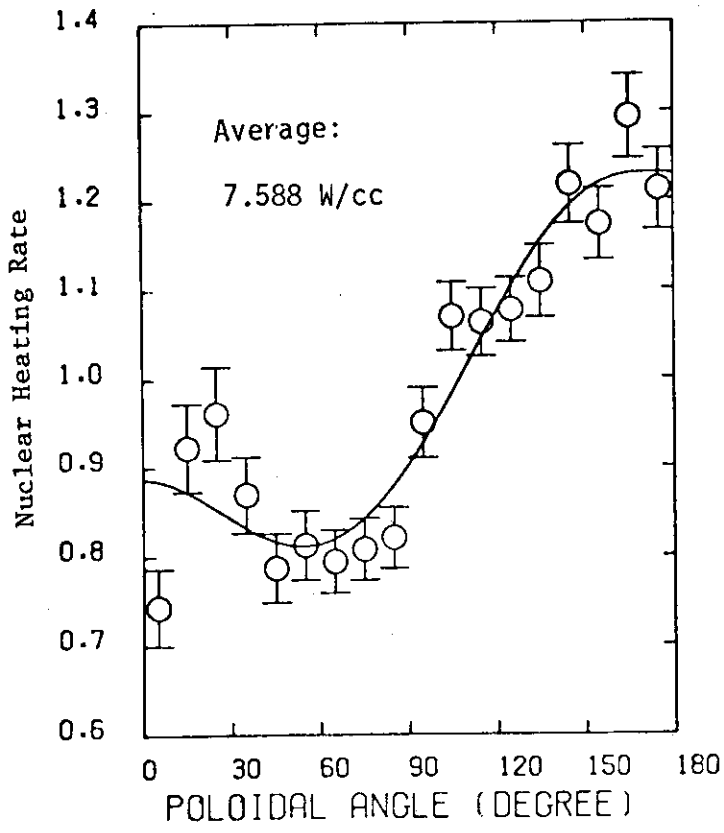

Fig.13 Poloidal distribution of Nuclear Heating Rate in the First Wall